Ground-based Parallax Confirmed by Spitzer

Document Version
Final published version

OPEN ACCESS

Ground-based Parallax Confirmed by *Spitzer*: Binary Microlensing Event MOA-2015-BLG-020

Tianshu Wang[1], Wei Zhu[2], Shude Mao[1,3,4], I. A. Bond[5], A. Gould[2,6,7], A. Udalski[8], T. Sumi[9], V. Bozza[10,11], C. Ranc[12], A. Cassan[13], J. C. Yee[14], C. Han[15], F. Abe[16], Y. Asakura[16], R. Barry[12], D. P. Bennett[12,17], A. Bhattacharya[12,17], M. Donachie[18], P. Evans[18], A. Fukui[19], Y. Hirao[9], Y. Itow[16], K. Kawasaki[9], N. Koshimoto[9], M. C. A. Li[18], C. H. Ling[5], K. Masuda[16], Y. Matsubara[16], S. Miyazaki[9], Y. Muraki[16], M. Nagakane[9], K. Ohnishi[20], N. Rattenbury[18], To. Saito[21], A. Sharan[18], H. Shibai[22], D. J. Sullivan[23], D. Suzuki[12,24], P. J. Tristram[25], T. Yamada[26], A. Yonehara[26]
(MOA Collaboration),
S. Kozłowski[27], P. Mróz[27], M. Pawlak[27], P. Pietrukowicz[27], R. Poleski[2,27], J. Skowron[27], I. Soszyński[27], M. K. Szymański[27], K. Ulaczyk[27]
(OGLE Collaboration),
C. Beichman[28], G. Bryden[29], S. Calchi Novati[10,30], S. Carey[31], M. Fausnaugh[2], B. S. Gaudi[2], C. B. Henderson[29], Y. Shvartzvald[29], B. Wibking[2]
(Spitzer Team),
M. D. Albrow[32], S.-J. Chung[6,33], K.-H. Hwang[34], Y. K. Jung[14], Y.-H. Ryu[6], I.-G. Shin[14], S.-M. Cha[6,35], D.-J. Kim[6], H.-W. Kim[6], S.-L. Kim[6,33], C.-U. Lee[6,33], Y. Lee[6,35], B.-G. Park[6,33], R. W. Pogge[2]
(KMTNet Collaboration),
and
R. A. Street[36], Y. Tsapras[37], M. Hundertmark[37], E. Bachelet[36,38], M. Dominik[39,43], K. Horne[39], R. Figuera Jaimes[39], J. Wambsganss[37], D. M. Bramich[44], R. Schmidt[37], C. Snodgrass[40], I. A. Steele[41], J. Menzies[42]
(RoboNet Collaboration)
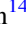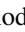
[1] Physics Department and Tsinghua Centre for Astrophysics, Tsinghua University, Beijing 100084, China; wts15@mails.tsinghua.edu.cn
[2] Department of Astronomy, Ohio State University, 140 West 18th Avenue, Columbus, OH 43210, USA
[3] National Astronomical Observatories, Chinese Academy of Sciences, 20A Datun Road, Chaoyang District, Beijing 100012, China
[4] Jodrell Bank Centre for Astrophysics, School of Physics and Astronomy, The University of Manchester, Oxford Road, Manchester M13 9PL, UK
[5] Institute of Natural and Mathematical Sciences, Massey University, Auckland 0745, New Zealand
[6] Korea Astronomy and Space Science Institute, 776 Daedeokdae-ro, Yuseong-Gu, Daejeon 34055, Korea
[7] Max-Planck-Institute for Astronomy, Königstuhl 17, D-69117 Heidelberg, Germany
[8] Warsaw University Observatory, AI. Ujazdowskie 4, 00-478 Warszawa, Poland
[9] Department of Earth and Space Science, Graduate School of Science, Osaka University, Toyonaka, Osaka 560-0043, Japan
[10] Dipartimento di Fisica "E. R. Caianiello," Universitá di Salerno, Via Giovanni Paolo II, I-84084 Fisciano (SA), Italy
[11] Istituto Internazionale per gli Alti Studi Scientifici (IIASS), Via G. Pellegrino 19, I-84019 Vietri Sul Mare (SA), Italy
[12] Code 667, NASA Goddard Space Flight Center, Greenbelt, MD 20771, USA; david.bennett@nasa.gov
[13] Sorbonne Universités, UPMC Univ Paris 6 et CNRS, UMR 7095, Institut d'Astrophysique de Paris, 98 bis bd Arago, F-75014 Paris, France
[14] Smithsonian Astrophysical Observatory, 60 Garden Street, Cambridge, MA 02138, USA
[15] Department of Physics, Chungbuk National University, Cheongju 361-763, Korea
[16] Institute for Space-Earth Environmental Research, Nagoya University, Nagoya 464-8601, Japan
[17] Department of Physics, University of Notre Dame, Notre Dame, IN 46556, USA
[18] Department of Physics, University of Auckland, Private Bag 92019, Auckland, New Zealand
[19] Okayama Astrophysical Observatory, National Astronomical Observatory of Japan, 3037-5 Honjo, Kamogata, Asakuchi, Okayama 719-0232, Japan
[20] Nagano National College of Technology, Nagano 381-8550, Japan
[21] Tokyo Metropolitan College of Aeronautics, Tokyo 116-8523, Japan
[22] Department of Earth and Space Science, Graduate School of Science, Osaka University, 1-1 Machikaneyama, Toyonaka, Osaka 560-0043, Japan
[23] School of Chemical and Physical Sciences, Victoria University, Wellington, New Zealand
[24] Institute of Space and Astronautical Science, Japan Aerospace Exploration Agency, Kanagawa 252-5210, Japan
[25] University of Canterbury Mt. John Observatory, P.O. Box 56, Lake Tekapo 8770, New Zealand
[26] Department of Physics, Faculty of Science, Kyoto Sangyo University, Kyoto 603-8555, Japan
[27] Warsaw University Observatory, Al. Ujazdowskie 4, 00-478 Warszawa, Poland
[28] NASA Exoplanet Science Institute, MS 100-22, California Institute of Technology, Pasadena, CA 91125, USA
[29] Jet Propulsion Laboratory, California Institute of Technology, 4800 Oak Grove Drive, Pasadena, CA 91109, USA
[30] IPAC, Mail Code 100-22,Caltech, 1200 East California Boulevard, Pasadena, CA 91125, USA
[31] Spitzer Science Center, MS 220-6, California Institute of Technology, Pasadena, CA, USA
[32] University of Canterbury, Department of Physics and Astronomy, Private Bag 4800, Christchurch 8020, New Zealand
[33] Korea University of Science and Technology, 217 Gajeong-ro, Yuseong-gu, Daejeon 34113, Korea
[34] Department of Physics, Institute for Astrophysics, Chungbuk National University, Cheongju 371-763, Korea
[35] School of Space Research, Kyung Hee University, Giheung-gu, Yongin, Gyeonggi-do, 17104, Korea
[36] Las Cumbres Observatory, 6740 Cortona Drive, Suite 102, Goleta, CA 93117, USA
[37] Zentrum für Astronomie der Universität Heidelberg, Astronomisches Rechen-Institut, Mönchhofstr. 12-14, D-69120 Heidelberg, Germany
[38] Qatar Environment and Energy Research Institute(QEERI), HBKU, Qatar Foundation, Doha, Qatar
[39] SUPA, School of Physics & Astronomy, University of St Andrews, North Haugh, St Andrews KY16 9SS, UK
[40] Planetary and Space Sciences, Department of Physical Sciences, The Open University, Milton Keynes, MK7 6AA, UK
[41] Astrophysics Research Institute, Liverpool John Moores University, Liverpool CH41 1LD, UK

[42] South African Astronomical Observatory, P.O. Box 9, Observatory 7935, South Africa

Abstract

We present the analysis of the binary gravitational microlensing event MOA-2015-BLG-020. The event has a fairly long timescale ($\sim$63 days) and thus the light curve deviates significantly from the lensing model that is based on the rectilinear lens-source relative motion. This enables us to measure the microlensing parallax through the annual parallax effect. The microlensing parallax parameters constrained by the ground-based data are confirmed by the *Spitzer* observations through the satellite parallax method. By additionally measuring the angular Einstein radius from the analysis of the resolved caustic crossing, the physical parameters of the lens are determined. It is found that the binary lens is composed of two dwarf stars with masses $M_1 = 0.606 \pm 0.028\,M_\odot$ and $M_2 = 0.125 \pm 0.006\,M_\odot$ in the Galactic disk. Assuming that the source star is at the same distance as the bulge red clump stars, we find the lens is at a distance $D_L = 2.44 \pm 0.10$ kpc. We also provide a summary and short discussion of all of the published microlensing events in which the annual parallax effect is confirmed by other independent observations.

Key words: binaries: general – Galaxy: bulge – gravitational lensing: micro

Supporting material: data behind figure

1. Introduction

In a microlensing event, companions to the primary lens object can be detected via their perturbations to the single-lens light curve (Mao & Paczynski 1991; Gould & Loeb 1992). From such perturbations, dimensionless parameters can be derived that are related to the binary system, such as the binary mass ratio q and the projected separation s (Gaudi & Gould 1997). Here, s is the instantaneous angular separation between the two components normalized to the angular Einstein radius

$$\theta_E \equiv \sqrt{\kappa M_L \pi_{rel}}, \tag{1}$$

where M_L is the total lens mass, and

$$\kappa \equiv \frac{4G}{c^2 \mathrm{au}} \approx 8.14\frac{\mathrm{mas}}{M_\odot}; \quad \pi_{rel} \equiv \mathrm{au}\left(\frac{1}{D_L} - \frac{1}{D_S}\right). \tag{2}$$

Here, π_{rel} is the lens-source relative parallax, and D_L and D_S are the distances to the lens and the source, respectively.

Although statistical conclusions can be drawn from measurements of q and s, the physical properties of the lens system, such as M_L, are of more interest. By far, the most popular way to convert from microlensing observables to physical quantities is to combine the measurements of θ_E and the microlensing parallax, $\pi_E \equiv \pi_{rel}/\theta_E$. Then,

$$M_L = \frac{\theta_E}{\kappa \pi_E}; \quad \pi_{rel} = \pi_E \theta_E. \tag{3}$$

There are several ways to measure θ_E (see a short summary given in Zhu et al. 2015), but the most common is to use the finite-source effect, which is the deviation in the light curve from the point-like source model due to the extended nature of the source star (Yoo et al. 2004).

For most published binary events, the microlensing parallax parameter π_E is measured through the annual parallax effect, in which Earth's acceleration around the Sun introduces deviations from rectilinear motion in the lens-source relative motion (Gould 1992). This method generically assumes that the lens (or lens system) and the source (or source system) are, or can be treated as, not undergoing acceleration. For binary lens

events, each component is under acceleration by the other, and this so-called lens orbital motion effect can be confused with the annual parallax effect (Batista et al. 2011).

Therefore, it is important to understand the validity of the annual parallax method for binary-lens events in practical use. This can be done by observing the binary system after the event, either photometrically (Dong et al. 2009; Bennett et al. 2010) or spectroscopically (Boisse et al. 2015; Yee et al. 2016). Another way is to measure π_E via the satellite parallax method (Refsdal 1966; Gould 1994). This is done by observing the same microlensing event from at least two well-separated locations; the difference between the light curves from these locations informs the parameter π_E. The microlensing parallax measured in this way is then determined independently from the orbital motion effect, and thus can be used to test the annual parallax method.

The *Spitzer* microlensing campaigns utilize the *Spitzer Space Telescope* to measure π_E via the satellite parallax method for hundreds of microlensing events (e.g., Calchi Novati et al. 2015a; Udalski et al. 2015; Yee et al. 2015a; Zhu et al. 2015). Of the several published binary events, OGLE-2015-BLG-0479, is found to have inconsistent π_E from the annual parallax and satellite parallax methods, and this inconsistency can be well explained by the full orbital motion of the lens system (Han et al. 2016). In the case of OGLE-2015-BLG-0196 and OGLE-2016-BLG-0168, the annual parallax effect is confirmed by the satellite parallax method (Han et al. 2017; Shin et al. 2017).

In this paper, we present the analysis of *Spitzer* binary event MOA-2015-BLG-020. This is the second published case in which the annual parallax effect agrees with the satellite parallax effect. We summarize the ground-based and space-based observations in Section 2, describe the light curve modeling in Section 3, and derive the physical properties of the binary system in Section 4. In Section 5, we review all of the published microlensing binaries in which the annual parallax effect has been confirmed or contradicted by other methods, and discuss the implications.

2. Observations

2.1. Ground-based Alert and Follow-up

At UT 10:06 on 2015 February 16 (HJD$' \equiv$ HJD $-$ 2450000 = 7101.87), the MOA collaboration identified the

microlensing event MOA-2015-BLG-020 at equatorial coordinates (R.A., decl.)$_{2000}$ = (17^{h}52^{m}52$\overset{s}{.}$78, −32°29′09″.1), with corresponding Galactic coordinates (l, b)$_{2000}$ = (−2°.24, −3°.16), based on data taken by its 1.8 m telescope with a 2.2 deg^2 field at Mt. John, New Zealand. These MOA observations were taken in a broad ~R+I bandpass at 15-minute cadence. The OGLE collaboration independently discovered this event about 2.5 days after the MOA alert. It was alerted as OGLE-2015-BLG-0102 through the OGLE Early Warning System (Udalski et al. 1994; Udalski 2003), based on observations from the 1.4 deg^2 camera on its 1.3 m Warsaw Telescope at the Las Campanas Observatory in Chile. This microlensing event lies in the OGLE-IV field BLG535 (Udalski et al. 2015), meaning that it received OGLE observations at a cadence of 2–3 observations per night.

Event MOA-2015-BLG-020 also lies in one of the four prime fields of the Korean Microlensing Telescope Network (KMTNet; Kim et al. 2016), and thus received dense coverage from KMTNet. In 2015, KMTNet observed a ~16 deg^2 prime microlensing field at ~10-minute cadence when the bulge was visible. The KMTNet consists of three 1.6 m telescopes, each equipped with a 4 deg^2 field of view camera. The observations started on 2015 February 3 (HJD′ = 7056.9) for its CTIO telescope, 2015 February 19 (HJD′ = 7072.6) for its SAAO telescope, and 2015 June 9 (HJD′ = 7182.9) for its SSO telescope, respectively.

This event was also observed by the Las Cumbres Observatory Network (LCO; Brown et al. 2013) to support the 2015 Spitzer microlensing campaign; see Street et al. (2016) for a more detailed description of the LCO observations. Between HJD′ = 7123.7 and 7174.8, event MOA-2015-BLG-020 received in total 186 observations from two 1 m telescopes at CTIO, 105 observations from two 1 m telescopes at SAAO, and 76 observations from two 1 m telescopes at SSO.

All ground-based data were reduced using the standard or variant version of the image subtraction method developed by Alard & Lupton (1998), employing a spatially variant kernel as necessary (see also Bramich 2008).

2.2. Spitzer Follow-up

Event MOA-2015-BLG-020 was selected for Spitzer IRAC 3.6 μm observations as part of the 2015 Spitzer microlensing campaign to probe the Galactic distribution of planets (Calchi Novati et al. 2015a; Zhu et al. 2017). The general description of the campaign and the target selection protocol can be found in Udalski et al. (2015) and Yee et al. (2015b), respectively. By the time the 2015 Spitzer program had started,[45] the binary nature of the current event had already been established. Therefore, it was selected as a "subjective binary" on 2015 June 1 (HJD = 2457175), meaning that Spitzer observations were taken specifically for the purpose of measuring the mass of the binary. Then observations started on 2015 June 8 (HJD = 2457182) and ended on 2015 July 15 (HJD = 2457219), when this target moved out of Spitzer's Sun-angle window. The cadences were determined objectively, and in total 61 observations were taken.

The Spitzer data were reduced by the software that was designed specifically for this microlensing program (Calchi Novati et al. 2015b). In the present case, because the source star is very bright and red, it was saturated on the Spitzer images

that were taken in the first few days. Although the saturation issue is in principle solvable (e.g., OGLE-2015-BLG-0763; Zhu et al. 2016), we decided to exclude the first 10 data points that are potentially affected by saturation, on the basis that no particularly interesting behavior occurred during this time interval. In the end, we include 51 Spitzer observations spanning from HJD′ = 7185.7 to 7221.8 for the parallax measurement.

3. Light Curve Modeling

3.1. Initial Solution Search

The light curve of event MOA-2015-BLG-020 suggests that it is a typical binary microlensing event (see Figure 1). In the standard terminology (i.e., binary event without parallax and lens orbital motion effects), the following seven parameters are used for characterizing a binary light curve: the time of the closest approach between the source and the binary lens (gravitational) center, t_0; the impact parameter normalized by the Einstein radius, u_0; the event timescale, t_E; the source size normalized by the Einstein radius, ρ; the projected separation between the binary components normalized to the Einstein radius, s; the binary mass ratio, q; and the angle between the binary-lens axis and the lens-source relative motion, α. There are two further flux parameters that describe the source flux (F_S^j) and the blending flux (F_B^j) for each observatory j that translate the magnification A to the observed flux at given time t_i

$$F^j(t_i) = F_S^j \cdot A(t_i) + F_B^j. \tag{4}$$

These flux parameters are found for each data set using linear fit. We use the the advanced contour integration code, `VBBinaryLensing`,[46] to compute of the binary lens magnification $A(t_i)$. This code includes a parabolic correction in Green's line integral, and can automatically adjust the step size of the integration based on the distance to the binary caustic, in order to achieve a desired precision in magnification. See Bozza (2010) for more details.

We start with a grid search on the ground-based data alone for the possible binary solution (or solutions). The grid search is conducted on parameters ($\log s$, $\log q$, $\log \rho$, α), with 16 values equally spaced between $−1 \leqslant \log s \leqslant 1$, $−3 \leqslant \log q \leqslant 0$, $−4 \leqslant \log \rho \leqslant 0$, and $0° \leqslant \alpha \leqslant 360°$, respectively. For each set of ($\log s$, $\log q$, $\log \rho$, α), we find the minimum χ^2 by going downhill on the remaining parameters (t_0, u_0, t_E).

The global minimum is found at $\log s \sim 0$ ($s \sim 1$), $\log q \sim −0.6$ ($q \sim 0.25$), $\log \rho \sim 2$, and $\alpha \sim 220°$, and there is no other locus on this grid that has similar χ^2.

We then refine the solution by performing Markov Chain Monte Carlo (MCMC) analysis around the initial solution found by the previous grid search, which employs the `emcee` ensemble sampler (Foreman-Mackey et al. 2013).

3.2. Inclusion of Microlensing Parallax Effect

The microlensing parallax effect has to be taken into account in order to simultaneously model the ground-based and space-based data. This effect invokes two additional parameters, $\pi_{E,N}$

---

[45] Although Spitzer observations did not start until 2015 June 8 (HJD = 2457182), the target selections started in late 2015 May.

[46] http://www.fisica.unisa.it/GravitationAstrophysics/VBBinaryLensing.htm
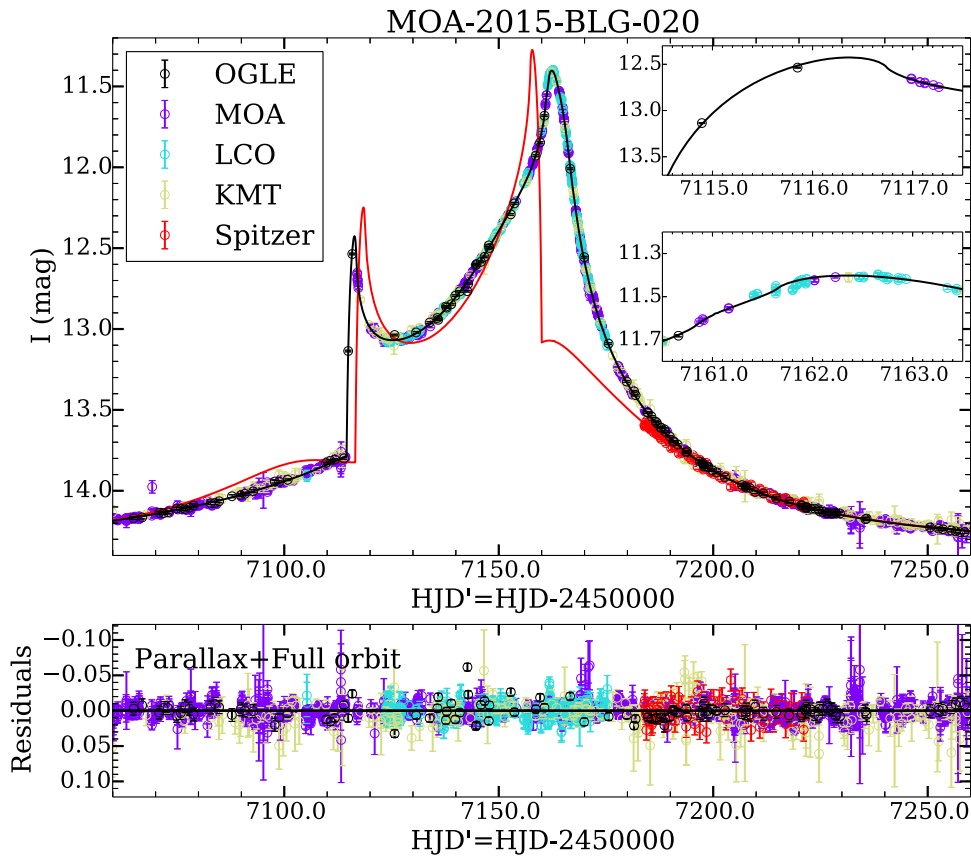
Figure 1. Light curve of event MOA-2015-BLG-020. In the top panel, the blue and red lines are the best-fit theoretical light curves for ground-based and satellite observations. The bottom panel shows the residual from the best model. Data points from different collaborations are shown with different colors. The data used to create this figure are available.

and $\pi_{E,E}$, which are the northern and eastern components of the parallax vector π_E.

We try to constrain π_E based on ground data alone, and by simultaneously modeling ground and *Spitzer* data, in order to check the consistency between annual parallax and satellite parallax effects. This check is possible here because MOA-2015-BLG-020 occurred relatively early in the season and had a fairly long timescale.

The annual parallax effect leads to two discrete solutions arising from the $\pm u_0$ degeneracy (e.g., Smith et al. 2003; Poindexter et al. 2005). In the case of MOA-2015-BLG-020, we find that the two solutions have $\Delta\chi^2 \geqslant 100$ because of strong annual parallax effect, indicating that the $+u_0$ solution is strongly favored over the $-u_0$ solution. We show in Figure 2 the 3-σ constraints on π_E based on ground-based data alone.

We then take into account the satellite parallax effect in order to include *Spitzer* data. We extract the geocentric locations of *Spitzer* during the entire season from the *JPL Horizons* website,[47] and project them onto the observer plane. The projected locations are then oriented and rescaled according to a given π_E to work out *Spitzer*'s view of the microlensing geometry.

We include the $I - [3.6\ \mu m]$ color constraint on the source star to better constrain the parallax parameters, considering the simple monotonic falling behavior of the *Spitzer* light curve. This has been demonstrated to be effective in single-lens cases

(e.g., Calchi Novati et al. 2015a; Zhu et al. 2017). The $I - [3.6\ \mu m]$ color constraint comes from putting the measured $V - I$ source color into the $I - [3.6\ \mu m]$ versus $V - I$ relation, which is derived based on a nearby field stars of similar colors (see Calchi Novati et al. 2015b for more details). This yields $I - [3.6\ \mu m] = 3.18 \pm 0.05$ mag. During the MCMC process, we calculate $I - [3.6\ \mu m]$ from the flux parameters (which are found using a linear fit), and reject any values that are $>3\sigma$ away from the central value.

The constraints on π_E from the simultaneous modeling of ground and *Spitzer* data are also shown in Figure 2. We note that these are the constraints from annual parallax and satellite parallax signals together. In order to separate constraints from these two types of parallaxes, we assume that the posteriors of the ground-only and ground+*Spitzer* fits are multivariate Gaussians, and derive the covariance matrix of the satellite parallax part (see the Appendix and Gould 2003) The derived matrix has a determinant that is statistically consistent with zero, which indicates a strong correlation between $\pi_{E,N}$ and $\pi_{E,E}$. This is because the *Spitzer* observations occasionally only measure a one-dimensional parallax component (see Shvartzvald et al. 2015 for a detailed discussion). We nevertheless proceed with the standard procedure and compute the difference between the annual parallax and the satellite parallax measurements, and find $\Delta\chi^2 = 11$. Although this would formally indicate a probability of $e^{-11/2} = 0.4\%$, it is actually well within
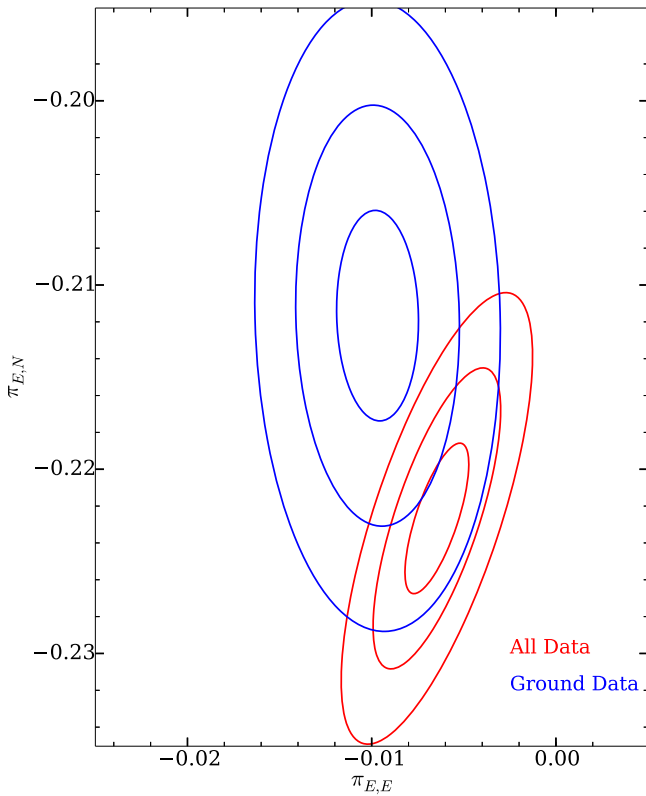
Figure 2. Distribution of microlensing parallax parameters $\pi_{E,E}$ and $\pi_{E,N}$ in the east and north directions. The red and blue contours are obtained based on the combined ground+*Spitzer* data and the ground data alone, respectively. The three contours show 1-σ ($\chi^2 = 1$), 2-σ ($\chi^2 = 4$), and 3-σ ($\chi^2 = 9$) confidence regions of the full orbit model.

the systematic uncertainty that the ground-based data can introduce.[48] Therefore, the small χ^2 indicates a good agreement between the annual parallax and the satellite parallax.

Notice that we took into account the four-fold parallax degeneracy (often denoted as $(++)$, $(+,-)$, $(-,+)$, and $(-,-)$). Two of these are eliminated since the $-u_0$ solution is excluded by the ground-based data, while the $(+,-)$ degeneracy from *Spitzer* is also eliminated.

3.3. Inclusion of Binary Lens Orbital Motion Effect

We then introduce the lens orbital motion effect into the light curve modeling. Despite the degeneracy between orbital motion and parallax, as we will see below, in this case this has no effect on the measured values or uncertainties of the parallax. We introduce orbital motion into the models in two different ways. First, we use the linear orbital motion approximation, which involves two parameters, $d\alpha/dt$ and ds/dt. For the binary system to remain bound, we also impose the constraints on the projected kinetic to potential energy ratio (Dong et al. 2009). Second, we also include z and dz/dt in addition to $d\alpha/dt$ and ds/dt, in order to account for the full Keplerian motion of the binary system. Here z and dz/dt quantify the binary separation (normalized to the Einstein radius) along the line of sight and its time derivative, respectively. See Skowron et al. (2011) for the conversion between these phase-space parameters and Keplerian

parameters. This conversion requires an input of the source angular size $\theta_\star$ in order to set the absolute physical scale, and we use $\theta_\star = 23.9\ \mu$as (see Section 4). Once the Keplerian parameters are derived, we check the orbital period P and reject any solution with $P_{orb} \geqslant 200$ years, in order to avoid the influence of systematics in the data.

The results of two modelings with different treatment of the orbital motion are given in Table 1; the triangle diagram of the fitting parameters for the full orbital model is shown in Figure 3. The source trajectories and caustics of the full orbit motion are shown in Figure 4. This solution has slightly worse χ^2 than the linear orbital motion solution, even though the former has two more free parameters. This is because the linear orbit solution (with the ratio of the perpendicular kinetic energy to the potential energy, $\beta = KE_{perp}/PE = 0.145$) has preferentially long orbital periods ($P_{orb} \gg 200$ years) for the binary system, which are not allowed in the full orbit solution. Nevertheless, the microlensing parameters (especially the microlens parallax) are stable regardless of whether and how the lens orbital motion is included.

4. Physical Parameters

We estimate the angular size of the source following the standard procedure (Yoo et al. 2004). First, we measure the centroid of the red clump in the OGLE $(V − I, I)$ color–magnitude diagram (CMD) of the stars within $2' \times 2'$ of our event (see Figure 5). By using stars in the box $1.8 < V − I < 2.4$ and $15.5 < I < 16.5$, we find the centroid of the red clump to be $(V − I, I)_{RC} = (2.11 \pm 0.05, 16.05 \pm 0.11)$. This, when combined with the instrumental color and magnitude of the source star $(V − I, I)_{S,OGLE} = (2.87, 14.34)$, yields an offset of $\Delta(V − I, I)_{OGLE} = (V − I, I)_{S,OGLE} − (V − I, I)_{RC,OGLE} = (0.76, −1.71)$. After applying the correction of the non-standard V band of OGLE-IV (Udalski et al. 2015; Zhu et al. 2015) $\Delta(V − I)_{JC} = \Delta(V − I)_{OGLE} \times 0.92 = 0.70$ (in which "JC" represents the standard Johnson-Cousins system) and adapting the intrinsic color and magnitude of the clump $(V − I, I)_{RC,0} = (1.06, 14.56)$ (Bensby et al. 2013; Nataf et al. 2013), we find that the intrinsic color and magnitude of source is $(V − I, I)_{S,0} = \Delta(V − I, I)_{JC} + (V − I, I)_{RC,0} = (1.76, 12.85)$.

To determine the source angular size, we employ the color-surface brightness relation of giant stars from Kervella et al. (2004), and finally find

$$\theta_\star = 23.9 \pm 1.0\ \mu\text{as.} \tag{5}$$

Therefore,

$$\theta_E = 1.329 \pm 0.049\ \text{mas.} \tag{6}$$

Then we obtain the total mass of the system using Equation (3):

$$M = 0.731 \pm 0.034\ M_\odot. \tag{7}$$

Combined with the mass ratio from our fit, we find that the lens system is a binary of $0.606\ M_\odot$ and $0.125\ M_\odot$. The lens-source relative parallax is $\pi_{rel} = 0.296 \pm 0.017$ mas, indicating a disk binary. Under the assumption that the source is at the same distance as the red clump centroid at this location ($D_S = 8.8$ kpc, Nataf et al. 2013), the distance to the lens is

$$D_L = 2.44 \pm 0.10\ \text{kpc.} \tag{8}$$

The lensing binary is vertically about 120 pc away from the Galactic plane, likely from the thin disk.

---

[48] In other words, we would never consider it a reliable parallax measurement if the annual parallax only has $\Delta\chi^2 = 11$ improvement compared to the standard model.
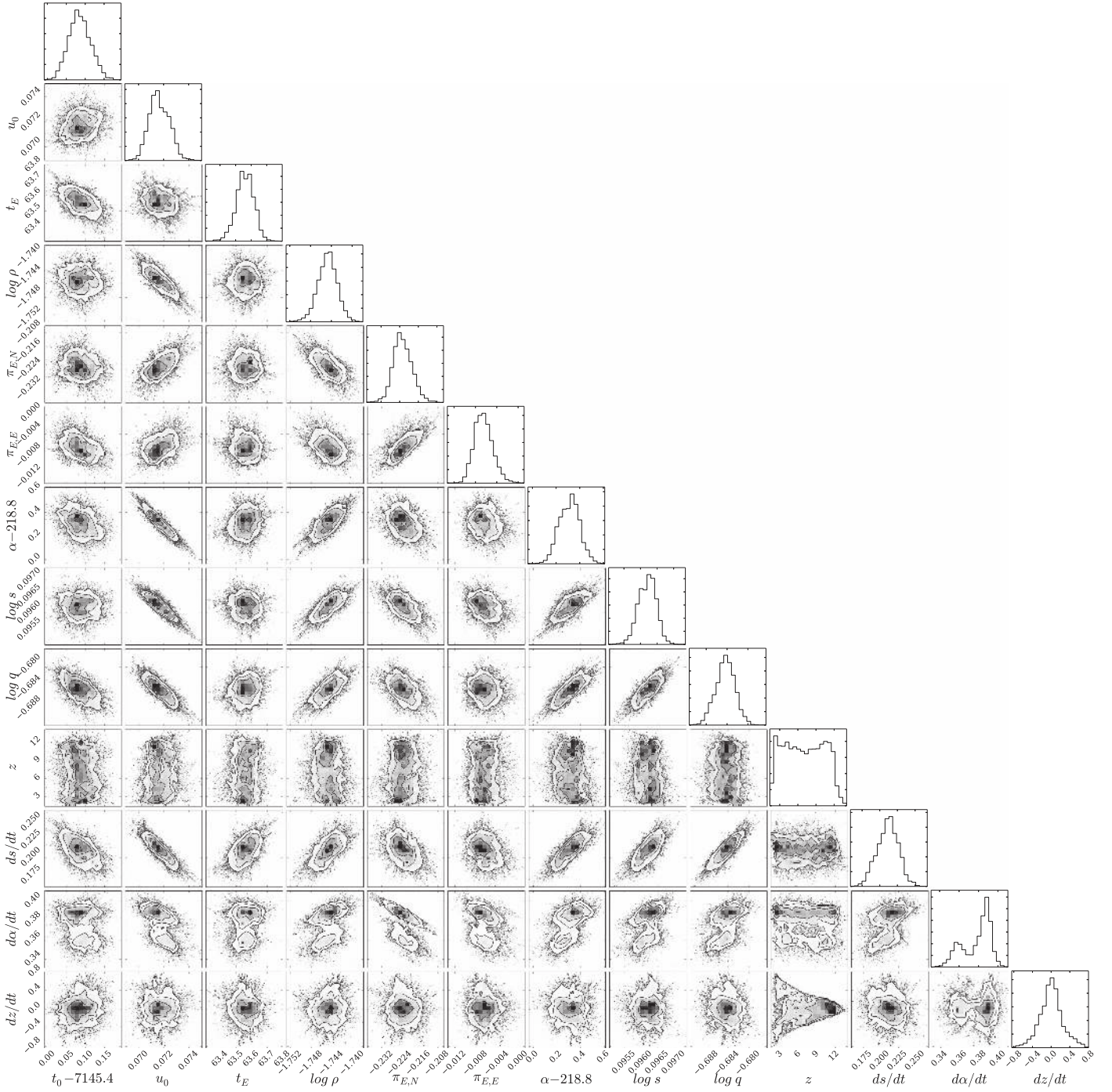
Figure 3. Triangle plot of the full orbit model with both ground-based and space-based data included in the fit. The orbital parameters (especially z) are not constrained as well as the standard microlensing parameters. Notice that the bimodal distribution of $\frac{d\alpha}{dt}$ is caused by excluding samples with a very long period (millions of years). Without such an exclusion, there would be only one peak.

The binary components are separated in projection by

$$r_\perp = 4.04 \pm 0.23 \text{ au.} \qquad (9)$$

We summarize the physical parameters in Table 2.

5. Discussion

We analyzed the binary-lensing event MOA-2015-BLG-020, which was observed both from the ground and from the *Spitzer Space Telescope*. The light curve from ground-based observations significantly deviated from the lensing model based on

the rectilinear lens-source relative motion, and we measured the microlensing parallax from the analysis of the deviation. The measured parallax was confirmed by the *Spitzer* data, showing the consistency between annual parallax and satellite parallax effects. By additionally measuring the angular Einstein radius from the analysis of the resolved caustic crossing, the mass and distance to the lens are determined. We find that the lens is a binary composed of two low-mass stars located in the Galactic disk. In our analysis, we find that the linear orbit model and full orbit model can fit the data almost equally well. Although the full orbit parameters z and dz/dt are not well constrained, we

Table 1
Best-fit Parameters

Parameters[a]	Ground+*Spitzer*			Ground-only			
	Full Orbit	Linear Orbit	Parallax Only	Full Orbit	Linear Orbit	Parallax Only	Without Parallax
χ^2/dof	4003.5/4028	4000.8/4030	4222.4/4032	3940.1/3967	3936.4/3969	4162.0/3971	5907.2/3973
$\log s$	0.0962 ± 0.0003	0.0963 ± 0.0003	0.0940 ± 0.0002	0.0962 ± 0.0003	0.0963 ± 0.0003	0.0940 ± 0.0002	0.08767 ± 0.00009
$\log q$	-0.684 ± 0.002	-0.683 ± 0.002	-0.703 ± 0.001	-0.685 ± 0.002	-0.685 ± 0.002	-0.703 ± 0.001	-0.7477 ± 0.0007
u_0	0.0716 ± 0.0008	0.0715 ± 0.0008	0.0798 ± 0.0004	0.0711 ± 0.0008	0.0715 ± 0.0008	0.0799 ± 0.0004	0.09109 ± 0.00015
t_0	7145.48 ± 0.03	7145.46 ± 0.03	7145.72 ± 0.03	7145.48 ± 0.03	7145.51 ± 0.03	7145.71 ± 0.03	7145.66 ± 0.01
t_E (days)	63.56 ± 0.06	63.55 ± 0.06	62.94 ± 0.06	63.74 ± 0.07	63.61 ± 0.08	62.94 ± 0.06	64.69 ± 0.03
$\log \rho$	-1.745 ± 0.002	-1.744 ± 0.002	-1.757 ± 0.002	-1.746 ± 0.002	-1.745 ± 0.002	-1.757 ± 0.002	-1.7969 ± 0.0009
α (deg)	219.12 ± 0.08	219.14 ± 0.08	218.27 ± 0.05	219.18 ± 0.08	219.14 ± 0.09	218.28 ± 0.05	217.43 ± 0.03
$\pi_{E,N}$	-0.223 ± 0.004	-0.223 ± 0.005	-0.220 ± 0.006	-0.212 ± 0.006	-0.211 ± 0.010	-0.218 ± 0.006	...
$\pi_{E,E}$	-0.007 ± 0.002	-0.006 ± 0.002	0.003 ± 0.002	-0.010 ± 0.002	-0.010 ± 0.002	0.003 ± 0.002	...
$\frac{ds}{dt}$ (year^{-1})	0.212 ± 0.015	0.217 ± 0.017	...	0.240 ± 0.017	0.225 ± 0.018	...	...
$\frac{d\alpha}{dt}$ (rad/year)	0.383 ± 0.014	-1.197 ± 0.038	...	0.371 ± 0.017	-1.197 ± 0.040	...	...
z	7.03 ± 3.17	...	...	4.78 ± 4.52	...	...	...
$\frac{dz}{dt}$ (year^{-1})	0.037 ± 0.258	...	...	0.277 ± 0.270	...	...	...
$V - I$	2.875 ± 0.003	2.874 ± 0.003	2.867 ± 0.003	2.876 ± 0.003	2.874 ± 0.003	2.868 ± 0.002	2.860 ± 0.002

Note.
[a] We use $\theta_* = 23.9$ μas in our full orbit model.
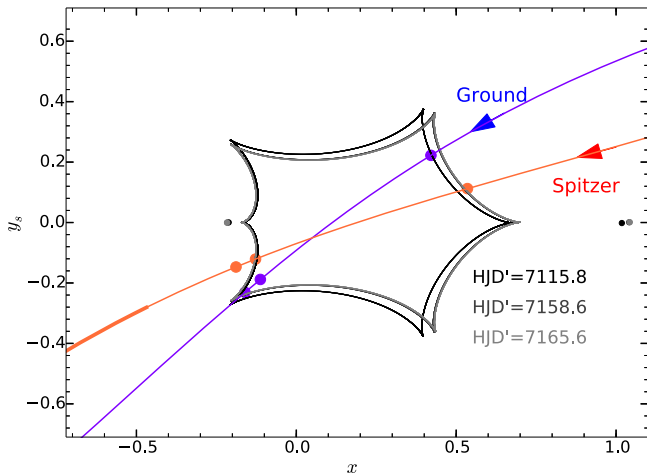
Figure 4. Caustics patterns for the event MOA-2015-BLG-020. Three caustic curves are shown for three different epochs (caustic entrance from the ground, caustic exits from *Spitzer* and ground), although the two at $HJD' = 7158.6$ and 7165.6 almost overlap. The corresponding lens and source positions are shown as solid dots. The source trajectories for the ground and *Spitzer* are shown as blue and red curves, respectively. The arrows indicate the directions of the source motions. The bold line segment indicates the epochs of the *Spitzer* data.
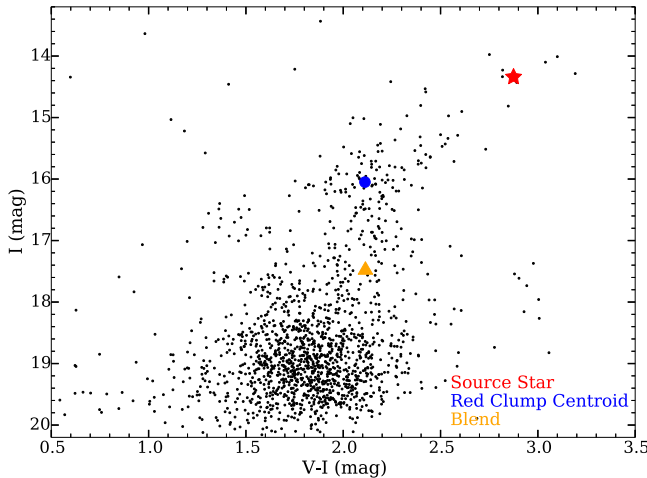
Figure 5. OGLE-IV calibrated color–magnitude diagram of the stars (black dots) within $2' \times 2'$ of MOA-2015-BLG-020/OGLE-2015-BLG-0102. The blue dot shows the centroid of the red clump stars. The red asterisk indicates the position of the microlensed source, and the yellow triangle shows the position of the blended object.

Table 2
Physical Parameters of the Binary Lens System MOA-2015-BLG-020

Parameters	
θ_E (mas)	1.329 ± 0.049
π_{rel} (mas)	0.296 ± 0.017
M_1 ($M_\odot$)	0.606 ± 0.028
M_2 ($M_\odot$)	0.125 ± 0.006
Distance to lens (kpc)	2.44 ± 0.10
Projected separation (au)	4.04 ± 0.23
Geocentric proper motion (mas yr^{-1})	7.64 ± 0.28

report lens physical parameters based on the full orbit model because of its physical foundation (Han et al. 2016).

The binary-lensing event MOA-2015-BLG-020 is peculiar in one aspect. Usually, the light curve for a caustic-crossing binary event has one sharp rise and one sharp fall during the

caustic entrance and exit, respectively, producing a "U"-shaped light curve. However, for this binary event, the caustic exit gracefully merges with the cusp crossing (see Figure 4), which causes the absence of the sharp decline in the ground-based light curve. This is almost a direct result of lens orbital motion. Note that this sharp decline is predicted to be present in the space-based light curve, but it is not observable by *Spitzer* due to various observational constraints (see Udalski et al. 2015 for details).

In Table 3, we summarize the published microlensing binaries in which the parallax parameters detected from ground (through annual parallax effect) are tested by other methods. The parallax parameters based on ground data in OGLE-2011-BLG-0417 and OGLE-2015-BLG-0479 seem to be inconsistent with the results of independent checks. Although there is still the possibility that the parallax detected by microlensing is wrong, it is believed that the radial velocity measurements for OGLE-2011-BLG-0417 do not test the parallax model. The reason is that the blended light of OGLE-2011-BLG-0417 is not the lens because it is brighter than predicted flux from the lens. The inconsistency in OGLE-2015-BLG-0479 is expected because of the strong lens orbital motion effect. Indeed, it is because of this inconsistency that the full Keplerian parameters of the binary in OGLE-2015-BLG-0479 can be well constrained (Han et al. 2016).

For the remaining events, the microlensing parallax parameters from the annual parallax effect are confirmed by additional observations (high-resolution imaging, radial velocity, or satellite parallax). As expected, they all have relatively long timescales ($t_E \gtrsim 60$ days), and the majority of them peaked (as seen from ground) either early (before May) or late (after August) in the microlensing season. Among these events, half are confirmed by ground observations (adaptive optics or radial velocity) and they all have a small impact parameter u_0, while those confirmed by satellite observations could have larger u_0 (modest magnification). This highlights *Spitzer*'s power to discover parallax events for moderately magnified events. The abundance of stellar binaries with $-1 \leqslant \log q \leqslant 0$ is roughly uniform as a function of $\log q$ ($dN/dq \propto q^{-1}$), consistent with Trimble (1990), although we caution that the number of events is small and no selection effects have been taken into account. As more and more lenses with definite masses are determined from microlensing, it will be very interesting to study these statistics much more carefully in the future.

Table 3
Summary of Events that have Annual Parallax Tested by Other Measurements

Event Name	Confirmed?	$(\pi_{E,N}, \pi_{E,E})$	Mass Ratio(s)	t_E (day)	t_0(HJD′)	u_0	I_S	$\Delta\chi^2_{parallax}$	$\Delta\chi^2_{orbit}$	References
High-resolution Imaging										
OGLE-2005-BLG-071	Yes	$(-0.30^{+0.24}_{-0.28}, -0.26 \pm 0.05)$	1.3×10^{-4}	71.1	3480.7 (04/20)	0.0282	19.5	<100	⋯	1, 2
OGLE-2006-BLG-109	Yes	$(-0.316 \pm 0.013, 0.139 \pm 0.006)$	$(1.4, 0.5) \times 10^{-3}$	128.1	3831.0 (04/05)	0.00345	20.9	13.5	⋯	3, 4
OGLE-2007-BLG-349	Yes	0.204 ± 0.034[a]	$(3.4 \times 10^{-4}, 0.49)$	118	4348.7 (09/05)	−0.00198	20.4	153	⋯	5
Radial Velocity:										
OGLE-2009-BLG-020	Yes	$(-0.022 \pm 0.086, 0.149 \pm 0.010)$	0.273	76.9	4917.3 (03/26)	0.0613	16.4	⋯	26.3	6, 7
OGLE-2011-BLG-0417	No	$(0.375 \pm 0.015, -0.133 \pm 0.003)$	0.292	92.3	5813.3 (09/08)	−0.0992	⋯	2024	656	8, 9, 10
Satellite Parallax:[b]										
OGLE-2014-BLG-0124	Yes	$(0.018 \pm 0.012, 0.108 \pm 0.023)$	0.752×10^{-3}	131	6836.2 (06/27)	0.2099	18.6	⋯	⋯	11
OGLE-2015-BLG-0479[c]	No[d]	$(-0.06 \pm 0.01, -0.11 \pm 0.01)$	0.81	86.3	7166.4 (05/23)	0.417[c]	19.6	⋯	43.5	12
OGLE-2015-BLG-0196	Yes	$(0.198 \pm 0.016, 0.100 \pm 0.009)$	0.99	96.7	7115.5 (04/03)	−0.037	15.9	2527.6	24.4	13
OGLE-2016-BLG-0168	Yes	$(0.382 \pm 0.022, 0.057 \pm 0.011)$	0724	97.0	7492.5 (04/13)	−0.201	19.5	159.4	115.04	14
MOA-2015-BLG-020	Yes	$(-0.223 \pm 0.005, -0.007 \pm 0.002)$	0.207	63.6	7145.5 (05/03)	0.0716	14.3	1983.5	218.9	This work

Notes.
[a] Bennett et al. (2016) used a different parameterization, with which the amplitude of the parallax vector was constrained.
[b] The microlens parameters are all from ground-based detection unless otherwise stated. The color, magnitude, and $\Delta\chi^2$ are from the combination of ground and satellite data sets.
[c] Parameters of OGLE-2015-BLG-0479 are from the analysis of the combination data set.
[d] That the full orbital motion is detectable in this event is noticeable based purely on the ground-based data. Therefore, this inconsistency is expected.

References. 1. Udalski et al. (2005), 2. Dong et al. (2009), 3. Gaudi et al. (2008), 4. Bennett et al. (2010), 5. Bennett et al. (2016), 6. Skowron et al. (2011), 7. Yee et al. (2016), 8. Shin et al. (2012), 9. Boisse et al. (2015), 10. Santerne et al. (2016), 11. Udalski et al. (2015), 12. Han et al. (2016), 13. Han et al. (2017), 14. Shin et al. (2017).

Appendix

Let a and c denote a parallax measurement and its covariance matrix, and the subscripts "comb" and "ground" indicate quantities appropriate for the combined and ground-based data. For example, $a_{\rm comb}$ and $c_{\rm comb}$ are the measured parallax and its covariance matrix from our MCMC fits for the combined data. We follow Gould (2003) to derive the "Spitzer" parallax and the consistency between the ground and Spitzer parallaxes (expressed as $\Delta\chi^2$) through the following steps. First, we introduce several quantities for later use

$$b_{\rm comb} = (c_{\rm comb})^{-1}, \, b_{\rm ground} = (c_{\rm ground})^{-1},$$
$$(d_{\rm comb})_i = \sum_j (b_{\rm comb})_{ij} \times (a_{\rm comb})_j,$$
$$(d_{\rm ground})_i = \sum_j (b_{\rm ground})_{ij} \times (a_{\rm ground})_j.$$

Then we calculate the corresponding quantities for the *Spitzer* parallax

$$b_{\rm spitzer} = b_{\rm comb} - b_{\rm ground}, \, d_{\rm spitzer} = d_{\rm comb} - d_{\rm ground},$$
$$c_{\rm spitzer} = (b_{\rm spitzer})^{-1},$$
$$(a_{\rm spitzer})_i = \sum_j (c_{\rm spitzer})_{ij} \times (d_{\rm spitzer})_j.$$
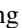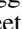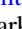
Finally, we compute the difference between the annual and satellite parallax measurements

$$\Delta\chi^2 = \sum_{ij} (a_{\rm diff})_i \times (b_{\rm diff})_{ij} \times (a_{\rm diff})_j,$$

where

$$a_{\rm diff} = a_{\rm ground} - a_{\rm spitzer},$$
$$c_{\rm diff} = c_{\rm ground} + c_{\rm spitzer},$$
$$b_{\rm diff} = (c_{\rm diff})^{-1}.$$

ORCID iDs

Wei Zhu https://orcid.org/0000-0003-4027-4711
Shude Mao https://orcid.org/0000-0001-8317-2788
V. Bozza https://orcid.org/0000-0003-4590-0136
J. C. Yee https://orcid.org/0000-0001-9481-7123
C. Han https://orcid.org/0000-0002-2641-9964
D. P. Bennett https://orcid.org/0000-0001-8043-8413
A. Fukui https://orcid.org/0000-0002-4909-5763
Y. Itow https://orcid.org/0000-0002-8198-1968
N. Rattenbury https://orcid.org/0000-0001-5069-319X
S. Kozłowski https://orcid.org/0000-0003-4084-880X
P. Pietrukowicz https://orcid.org/0000-0002-2339-5899
J. Skowron https://orcid.org/0000-0002-2335-1730
S. Calchi Novati https://orcid.org/0000-0002-7669-1069
S. Carey https://orcid.org/0000-0002-0221-6871
B. S. Gaudi https://orcid.org/0000-0003-0395-9869
C. B. Henderson https://orcid.org/0000-0001-8877-9060
Y. Shvartzvald https://orcid.org/0000-0003-1525-5041
M. D. Albrow https://orcid.org/0000-0003-3316-4012
S.-J. Chung https://orcid.org/0000-0001-6285-4528
Y.-H. Ryu https://orcid.org/0000-0001-9823-2907
I.-G. Shin https://orcid.org/0000-0002-4355-9838
R. W. Pogge https://orcid.org/0000-0003-1435-3053
R. A. Street https://orcid.org/0000-0001-6279-0552
Y. Tsapras https://orcid.org/0000-0001-8411-351X
M. Hundertmark https://orcid.org/0000-0003-0961-5231
M. Dominik https://orcid.org/0000-0002-3202-0343
K. Horne https://orcid.org/0000-0003-1728-0304
J. Wambsganss https://orcid.org/0000-0002-8365-7619
C. Snodgrass https://orcid.org/0000-0001-9328-2905
I. A. Steele https://orcid.org/0000-0001-8397-5759

References

Alard, C., & Lupton, R. H. 1998, ApJ, 503, 325
Batista, V., Gould, A., Dieters, S., et al. 2011, A&A, 529, A102
Bennett, D. P., Rhie, S. H., Nikolaev, S., et al. 2010, ApJ, 713, 837
Bennett, D. P., Rhie, S. H., Udalski, A., et al. 2016, AJ, 152, 125
Bensby, T., Yee, J. C., Feltzing, S., et al. 2013, A&A, 549, A147
Boisse, I., Santerne, A., Beaulieu, J.-P., et al. 2015, A&A, 582, L11
Bozza, V. 2010, MNRAS, 408, 2188
Bramich, D. M. 2008, MNRAS, 386, L77
Brown, T. M., Baliber, N., Bianco, F. B., et al. 2013, PASP, 125, 1031
Calchi Novati, S., Gould, A., Udalski, A., et al. 2015a, ApJ, 804, 20
Calchi Novati, S., Gould, A., Yee, J. C., et al. 2015b, ApJ, 814, 92
Dong, S., Gould, A., Udalski, A., et al. 2009, ApJ, 695, 970
Foreman-Mackey, D. 2016, JOSS, 1, 24
Foreman-Mackey, D., Hogg, D. W., Lang, D., & Goodman, J. 2013, PASP, 125, 306
Gaudi, B. S., Bennett, D. P., Udalski, A., et al. 2008, Sci, 319, 927
Gaudi, B. S., & Gould, A. 1997, ApJ, 486, 85
Gould, A. 1992, ApJ, 392, 442
Gould, A. 1994, ApJL, 421, L75
Gould, A. 2003, arXiv:astro-ph/0310577v1
Gould, A., & Loeb, A. 1992, ApJ, 396, 104
Han, C., Udalski, A., Gould, A., et al. 2016, ApJ, 828, 53
Han, C., Udalski, A., Gould, A., et al. 2017, ApJ, 834, 82
Kervella, P., Bersier, D., Mourard, D., et al. 2004, A&A, 428, 587
Kim, S.-L., Lee, C.-U., Park, B.-G., et al. 2016, JKAS, 49, 37
Mao, S., & Paczynski, B. 1991, ApJL, 374, L37
Nataf, D. M., Gould, A., Fouqué, P., et al. 2013, ApJ, 769, 88
Poindexter, S., Afonso, C., Bennett, D. P., et al. 2005, ApJ, 633, 914
Refsdal, S. 1966, MNRAS, 134, 315
Santerne, A., Beaulieu, J.-P., Rojas Ayala, B., et al. 2016, A&A, 595, L11
Shin, I.-G., Han, C., Choi, J.-Y., et al. 2012, ApJ, 755, 91
Shin, I.-G., Udalski, A., Yee, J. C., et al. 2017, ApJ, submitted (arXiv:1706.00499)
Shvartzvald, Y., Udalski, A., Gould, A., et al. 2015, ApJ, 814, 111

Skowron, J., Udalski, A., Gould, A., et al. 2011, ApJ, 738, 87
Smith, M. C., Mao, S., & Paczyński, B. 2003, MNRAS, 339, 925
Street, R. A., Udalski, A., Calchi Novati, S., et al. 2016, ApJ, 819, 93
Trimble, V. 1990, MNRAS, 242, 79
Udalski, A. 2003, AcA, 53, 291
Udalski, A., Jaroszyński, M., Paczyński, B., et al. 2005, ApJL, 628, L109
Udalski, A., Szymanski, M., Kaluzny, J., et al. 1994, AcA, 44, 227
Udalski, A., Szymański, M. K., & Szymański, G. 2015, AcA, 65, 1

Udalski, A., Yee, J. C., Gould, A., et al. 2015, ApJ, 799, 237
Yee, J. C., Gould, A., Beichman, C., et al. 2015, ApJ, 810, 155
Yee, J. C., Johnson, J. A., Skowron, J., et al. 2016, ApJ, 821, 121
Yee, J. C., Udalski, A., Calchi Novati, S., et al. 2015, ApJ, 802, 76
Yoo, J., DePoy, D. L., Gal-Yam, A., et al. 2004, ApJ, 603, 139
Zhu, W., Calchi Novati, S., Gould, A., et al. 2016, ApJ, 825, 60
Zhu, W., Udalski, A., Calchi Novati, S., et al. 2017, arXiv:1701.05191
Zhu, W., Udalski, A., Gould, A., et al. 2015, ApJ, 805, 8